ZnO/Ag/ZnO Multilayers as an n-type Transparent Conducting Electrode for Transparent Organic Light-Emitting Diodes

Sneha Sreekumar[1], Vladimir Bruevich[3], Vitaly Podzorov[3], Deirdre O'Carroll[1,2]

[1]Department of Chemistry and Chemical Biology, Rutgers University, 123 Bevier Rd., Piscataway, NJ 08854, USA.

[2]Department of Materials Science and Engineering, Rutgers University, 607 Taylor Rd., Piscataway, NJ 08854, USA.

[3]Department of Physics and Astronomy, 136 Frelinghuysen Rd, Piscataway, NJ 08854, USA.

Abstract

Alternative transparent conducting electrodes (TCEs) have gained significant attention in recent decades in an effort to replace costly indium-tin oxide (ITO) in organic optoelectronic devices. For example, state-of-the-art top-emitting, transparent organic light-emitting diodes (OLEDs) in the display industry require a transparent or semi-transparent cathode for electron injection. The current OLED display technology employs ultrathin metallic (typically Mg:Ag) layers as semitransparent cathodes. However, recent studies have shown that metal oxide/metal/meta-oxide multiplayers can perform better optically and offer improved stability compared to semitransparent metal cathodes. Yet, deposition of these multilayers with minimal damage to the underlying organic emissive layer is imperative. Here, we investigate the ZnO/Ag/ZnO TCE system deposited under mild sputtering conditions that are safe for the emissive layer. We demonstrate ~85% transparent electrodes with a sheet resistance of 1.47 Ω/□, which is more conductive than the industry standard, ITO. We also integrated such a multilayer electrode in a transparent OLED device built on ITO, demonstrating the compatibility of this TCE with the existing OLED technology.

Key Words: zinc oxide, silver, multilayer, transparent conducting electrodes, transparent organic light-emitting diodes (TOLEDs)

1. Introduction

With its strong popularity in the field of energy efficiency and information technology, optoelectronics demands materials that can improve energy conversion at low energy cost. Organic light-emitting diodes (OLEDs) have emerged as the main display technology due their high color purity and quality, low power consumption, high brightness, wide color range and easy processability, with ultra-thin form factor and flexibility. Research related to transparent conducting electrode (TCE) materials plays a significant role in transmitting light and current throughout an OLED device efficiently. Most OLED devices are built on indium-doped tin oxide (ITO), which has low resistivity and good transparency. However, due to its high cost and embodied energy, as well as the shortage of indium, alternatives are needed. Commonly used alternative TCEs are carbon based materials like carbon nanotubes or graphene oxide composites, metal nanocomposites, or PEDOT:PSS (poly(3,4-ethylenedioxythiophene):poly(styrenesulfo[1]nate) based TCEs. These materials provide good conductivity but have other issues such as surface energy mismatch with the active layers or they are easily susceptible to surface degradation.

Another option is to use multilayers of transition metal oxides (TMOs) with a bandgap tuned by introducing another metal ion. For example, Al-doped ZnO is commonly used as a TCE in solar cells with its work function and conductivity varying as the Al content increases[1, 2]. Apart from doping, a metal layer can be incorporated in between two TMO layers such that it forms a TMO/metal/TMO multilayer. The advantage of this approach is that the thickness of the metal layer determines the conductivity and the transmittance of the TCE, in which the conductivity can be improved compared to doped oxides. The charges in the three layers rebalance due to band bending, and the whole multilayer TCE has a single effective work function. [2, 3]

Here, we study ZnO/Ag/ZnO multilayers as the top transparent n-type electrode in polymer-based OLED devices. The ZnO/Ag/ZnO multilayer can serve as an anti-reflection layer, Electron Transport Layer(ETL), and a capping layer. It seems to be a promising candidate due to ZnO's very good environmental stability, electron mobility and transparency in visible range[4]. In contrast to many earlier studies, we deposit the transparent multilayer on top of the emissive layer. This approach is applicable to device architectures such as top-emitting OLEDs and transparent OLEDs. There are numerous studies on sandwiching a metal, typically Ag, in between two layers of ZnO, where Ag is in planar form, or in the form of wires or a mesh[2, 5-11]. Depending on the thickness and interactions with the ZnO layer, the transmittance and conductivity of the multilayer vary. With Ag nanowires and Ag meshes, more than ~91% transparency at a sheet resistance of about 9 Ω/sq have been reported[9]. When there is a need to pattern the electrodes, especially for top-emitting OLEDs, methods are needed that are more compatible with the emissive layer. In that case, it is more practical to use a planar Ag layer in between ZnO and vary the sputtering conditions. Previous work done with ZnO/Ag/ZnO for ITO replacement has been able to achieve a transparency of more than 80% and a sheet resistance of 25 Ω/sq[7, 8] by exposing the TCE to swift heavy ion (SHI) radiation or by etching the Ag layer. Mohamed et.al optimized the ZnO and Ag layers to show a conductive TCE with a ~90% transparency and a sheet resistance of 2.3 Ω/sq at a sputtering condition of 500 mA[12]. As we increase the thickness of the Ag layer, the rate of film formation will change the localized surface plasmon resonance (LSPR) properties of the Ag, which will dictate the transmittance and the conductive properties of the multilayer. Here, we fabricate multilayers of ZnO/Ag/ZnO in mild sputtering conditions without breaking the vacuum and vary the thickness of Ag to find the optimal optical and electrical characteristics of the TCE. Although prior studies have reported use of such TCEs in thin-film solar cells[10, 13], there are very few reports of implementing ZnO/Ag/ZnO multilayers in OLEDs. From reports on perovskite solar cells (PSCs), ZnO-based multilayer electrode systems are shown to be more stable at higher annealing temperatures than indium-based multilayer electrode systems like ITO/Ag/ITO[14-17]. Liu et.al demonstrated using ZnO/Ag/ZnO layers deposited through atomic layer deposition (ALD) in a vacuum-deposited bottom-emitting OLED, while Chen et.al

demonstrated the use of a ZnO/Mg:Ag/ZnO TCE in transparent OLEDs[18, 19]. Kang et.al demonstrated the use of a Ni-doped multilayer of ZnO/Ag/ZnO as a replacement for ITO as cathode on PET substrates for bottom-emitting, thermally activated delayed fluorescence (TADF) OLEDs[20]. Here, we demonstrate n-type ZnO/Ag/ZnO with a very low sheet resistance and good transparency (>80%) deposited directly on the emissive layer and its function in a transparent OLED device. This study is relevant to top-emitting and transparent OLEDs, which are importance because of their potential incorporating into active-matrix OLEDs (AMOLEDs) and microdisplays where fabrication of efficient and robust TCEs through low-energy deposition methods are important to protect the underlying organic active layer from significant degradation due to radiation, charging or heating[19, 21].

2. Materials and Methods

2.1. Materials

Zinc oxide (ZnO)(99.9% purity, 7.62 cm diameter and 0.32 inch thick), silver (Ag)(99.9% purity, 7.62 cm diameter and 0.32 inch thick) sputtering targets and calcium (Ca), aluminium (Al) pellets were purchased from Kurt. J Lesker. ITO patterned substrates, PEDOT: PSS (Al4083), poly(9,9'-dioctylfluorene) (PFO, molecular weight, MW = 20 kDa) and poly(9,9-dioctylfluorene-alt-benzothiadiazole) (F8BT, molecular weight, MW = 20 kDa) were purchased from Ossila.

2.2. ZnO/Ag/ZnO Multilayer Fabrication

Glass substrates were cleaned in a soap water bath, deionized water (4 rinses), acetone and then isopropanol and dried with an air gun for multilayer fabrication. RF sputtering power was minimized by looking at the lowest sputtering rate possible (0.4 - 0.5 Å/s) to get a uniform film. 20 nm of ZnO was deposited by RF sputtering using an RF power of 100 W for 660 s keeping the argon flow rate of 30.1 cc/min and the chamber pressure 10^{-9} torr. An Ag layer was deposited on top of the first ZnO layer using DC sputtering, varying thickness between 5 nm and 15 nm by varying the sputtering time from 80 s to 150 s and keeping a sputtering current of 100 mA under an argon flow of 30.1 cc/min. A second 20 nm of

ZnO was deposited onto the Ag layer under the same conditions as the first ZnO layer. The rotation speed of the substrate was kept constant at 50 rpm throughout each sputter deposition step.

2.3. Device Fabrication

ITO substrates were cleaned in a soap water bath, deionized water (4 rinses), acetone, isopropanol and dried with an air gun. They were subjected to Ar/O_2 plasma treatment for 20 min. 30 µl of PEDOT: PSS was spin coated onto these substrates at a speed of 5000 rpm and annealed on a hot plate at 150 ^{o}C for 5 min. An emissive layer of PFO:F8BT (19:1) was spin coated from a 15 mg/mL solution in toluene in a nitrogen atmosphere glove box and annealed for 10 min. at 80 ^{o}C on a hotplate. Subsequently, 20 nm of ZnO, 15 nm of Ag, and 20 nm of ZnO were sputtered sequentially, using RF and DC sputtering for ZnO and Ag, respectively.

2.4. Characterization

Transmission spectra were recorded using a SI Photonics CCD Array UV-Visible spectrometer. Atomic force microscopy (AFM) measurements were performed using an Asylum Research Cypher ES atomic force microscope operating in amplitude modulation mode or "tapping mode" to obtain both phase and height images. Silicon cantilevers with a spring constant of 2 N/m, a frequency of 70 kHz and a tip radius of 7 nm were used for all measurements. A scan size of 1 μm^2 with a digital resolution of 256 lines × 256 points and a scan rate of 2.44 Hz were used. For Hall measurements, contacts in a Hall-bar geometry were hand-painted on top of the film using a conducting colloidal silver paint (12630, Electron Microscopy Systems). The photograph of the device is shown in the Supporting Information (Fig. S1c). Hall effect measurements in the optimized ZnO/Ag/ZnO film were carried out using a high-sensitivity custom-designed *ac*-Hall apparatus described in detail elsewhere.[22] The longitudinal (bias) current was controlled by a Keithley-6221 Current Source. Longitudinal (4-probe) voltage was measured with a Keithley-6514 Electrometer. The *ac*-Hall voltage was measured using a Stanford Research SR830 lock-in amplifier with a DL Instruments 1201 Preamplifier. The sample in a Hall-bar geometry (shown in Supporting

Information) was placed in a hermetic chamber filled with high-purity Argon gas. The frequency of the *ac* magnetic field was 0.3 Hz. The measured Hall mobility was found to be nearly independent of the frequency of the *ac* magnetic field or the magnitude of the current applied to the sample, as shown in Supporting Information (Fig. S1). Film thickness was measured using a The DektakXT® stylus profilometer. The X-ray photoelectron spectroscopy (XPS) measurements were carried out using a Thermo Scientific K-Alpha X-ray photoelectron spectrometer with a monochromatic Al Kα source (1486.6 eV), hemispherical analyzer, and multichannel detector. The measurements were taken at a takeoff angle of 90° with a 0.79 mm^2 spot size and at a pressure of $<10^{-8}$ mbar. Ultraviolet photoelectron spectroscopy (UPS) measurements were performed with a Thermo Scientific ESCALAB250 Xi using a He I source (21.2 eV) with a pass energy of 2 eV, dwell time of 50 ms and an energy step size of 0.1 eV.

Current density-voltage (JV) and luminance-voltage (LV) characteristics were measured using Kiethley-2400 source-measure unit coupled to Konica Minolta chromameter 200, and electroluminescence (EL) spectra were measured using a BWTEK TE-cooled array spectrometer connected to a CCSA1 diffuser from Thorlabs. The spectra were measured at 10 V with an acquisition time of 1 min. The luminance was assumed to following a Lambertian emission pattern and was corrected by a factor of to account for emission from both sides of the device. The photoluminescence (PL) spectra were measured using Horiba's Fluorolog-3 spectrofluorometer equipped with a 450 W xenon lamp source. PL emission was measured at 22.5° to the incident light path, which is the front face collection path. The dark-field scattering spectra were taken using a broadband Xenon Lamp coupled to a 50x microscope objective and using an exposure time of 2 s and 10 accumulations.

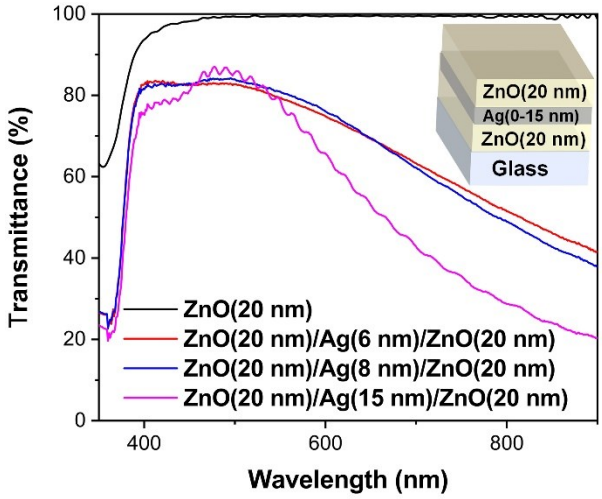

Figure 1. Optical transmittance spectra of ZnO/Ag/ZnO multilayers with 20 nm-thick ZnO and a varying thickness of Ag (6, 8, and 15 nm).

3. Results and Discussion

Sputter deposition provides a way to deposit thin films of metals and dielectrics on a substrate or active layer in the same instrument. Figure 1 shows the effect of varying the thickness of Ag in the ZnO/Ag/ZnO multilayer on electrical conductivity and transmittance. The transmittance spectra exhibit ripples that are caused by optical interference within the sample while aligning the substrate to the detector slit. The Ag thickness varied from 6 nm (based on the work done by Sahu et al.[11]) to 15 nm. We have found that on increasing the thickness to 15 nm with a sputtering time of 150 s and a sputtering current of 100 mA, the sheet resistance decreases considerably to 1.47 Ω/□ and the transmittance decreases from almost 100% (for ZnO) to 75-85% for ZnO/Ag/ZnO in the 400 nm to 600 nm wavelength range. As the Ag thickness increases the transmittance spectrum becomes narrower and a peak emerges at ~500 nm for the Ag thickness of 15 nm. This is attributed to increased scattering arising from localized surface plasmon resonances (LSPR) of larger Ag particles. Presence of LSPRs is also observed in the dark-field (DF) scattering spectra reported in Supporting Information Figure S2a, which shows scattering spectra as a

function of increasing Ag thickness. The scattering increases and is clearly visible for the multilayer with Ag having a thickness of 15 nm due to the formation of plasmonic Ag. The PL spectra shown in Figure S2b show mostly two types of emission: a UV-visible emission peak between 300-500 nm that corresponds to band edge emission of ZnO, and a weak visible emission peak between 600-800 nm that corresponds to oxygen vacancy defects[6]. The band edge emission due to the recombination of free excitons in pristine ZnO is at 380 nm[23], which shifts to 396 nm in the multilayers and not seen clearly for 20 nm of ZnO alone. There is a second shoulder at 440 nm, which is a blue emission band that could indicate electron transitions from interstitial Zn levels to the top of the valence band, and the energy levels of interstitial Zn-Zn vacancies[24]. The peaks due to oxygen vacancies, where recombination can occur with the electrons in the vacancies and photoexcited holes in the valence band, are very weak for the 6 nm Ag and disappear for 15 nm Ag, indicating a better charge balance for this multilayer. Ag films on ZnO as a function of Ag thickness are investigated through AFM imaging (Fig. 2a-d), and the root-mean-squared (RMS) roughness values were calculated. The RMS roughness of the ZnO is 3.6 ± 0.5 nm, which decreases on adding 6 nm of Ag to 1.8 ± 0.2 nm, and then further decreases with 8 nm of Ag to 1.4 ± 0.2 nm. For the 15 nm Ag films, RMS roughness increases to 3.1 ± 0.3 nm. The RMS roughness values go down on depositing Ag to a thickness of 8 nm, and then increases again for the multilayer with 15 nm of Ag, which is consistent with the formation of plasmonic Ag particles (also supported by the DF scattering spectra).

Table 1 shows Hall-effect measurements conducted on the multilayers to obtain mobility and charge carrier density. With increasing thickness of Ag interlayer, the mobility increases from 7.45 to 21. 2 $cm^2V^{-1}s^{-1}$, while the 3D charge carrier concentration does not show much of a systematic change, varying from 1.6×10^{23} cm^3 for an Ag thickness of 6 nm to 1.8×10^{23} cm^3 for 8 nm and reducing to 1.3×10^{23} cm^3 for 15 nm, which indicates that the sheet resistivity and conductivity are mostly governed by the carrier mobility. The Hall mobility is lower for thinner Ag layers due to an increased effect of inelastic charge scattering from the Ag/ZnO interfaces.[25, 26] The sheet resistance reduced from 7.88 Ω/□ to 1.47 Ω/□ by

varying the Ag thickness from 6 to 15 nm, which makes it a good electrode design. The figure of merit, ϕ_{TC}, in units of $\%\Omega^{-1}$ was calculated as the ratio between the transmittance (T) in percent and the sheet resistance (R) in Ω/□ and is given by $\phi_{TC} = \frac{T}{R}$.[27, 28] The figure of merit values calculated for the different multilayers are included in Table 1 and show a significant increase for the multilayer with Ag thickness of 15 nm. The hall mobilities and the transmittance spectra remained similar after measuring them 14 days later, which indicates that the electrode layers are stable.

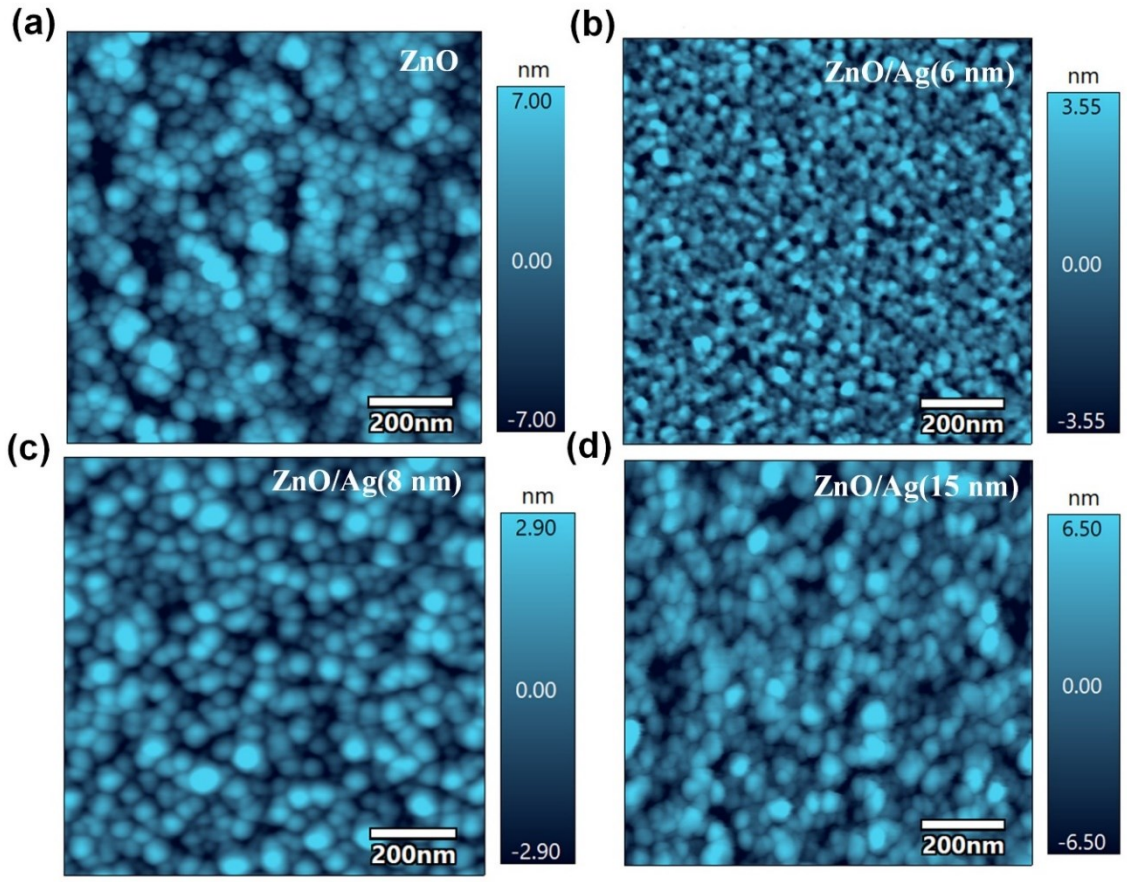

Figure 2. AFM images of the Ag layers of varied thickness (indicated) deposited on ZnO. The film roughness is shown by the height scale bar.

Table 1. Electric properties of different multilayers derived from Hall measurements.

Sample	Mobility ($cm^2V^{-1}s^{-1}$)	Conductivity (S/□)	Sheet Resistance (Ω/□)	Charge carrier density (cm^{-3})	Figure of merit ($\%\Omega^{-1}$)
ZnO/Ag (6 nm)/ ZnO	7.45	0.13	7.88	1.6×10^{23}	10.4
ZnO/Ag(8 nm)/ZnO	9.54	0.20	5.02	1.8×10^{23}	16.5
ZnO/Ag(15 nm)/ZnO	21.2	0.68	1.47	1.3×10^{23}	57.8

XPS spectra of Zinc shows peak Zn $2p_{3/2}$ and Zn $2p_{1/2}$ as shown in Figure 3a where, for the multilayers, the peaks appear at 1022.1 eV and 1045.2 eV, respectively. This is due to the presence of Zn^{2+} ions on the top surface of the multilayer. The shift in Zn $2p_{3/2}$ towards low binding energy in samples of ZnO/Ag indicates an increase of metallic Zn giving it a degenerate behavior which is indicative of transfer of electron from Ag species to Zinc resulting in the band bending at the interface.[7] Oxygen shows a peak at 532.38 eV which is present in all the spectra including the Si substrate which is due to atmospheric oxygen while the peak at ~530eV is indicative of O^{2-} ions in the hexagonal wurtzite structure of ZnO. A peak at ~529 eV which is due to AgO formation is absent in the spectra which means that the Ag surface remains pristine in the process. Looking at Ag spectra we see a doublet peak at 368.4 eV and 372 .4 eV for Ag $3d_{5/2}$ and Ag $3d_{3/2}$. There is a smaller peak at 371.9 eV and 377.48 eV.

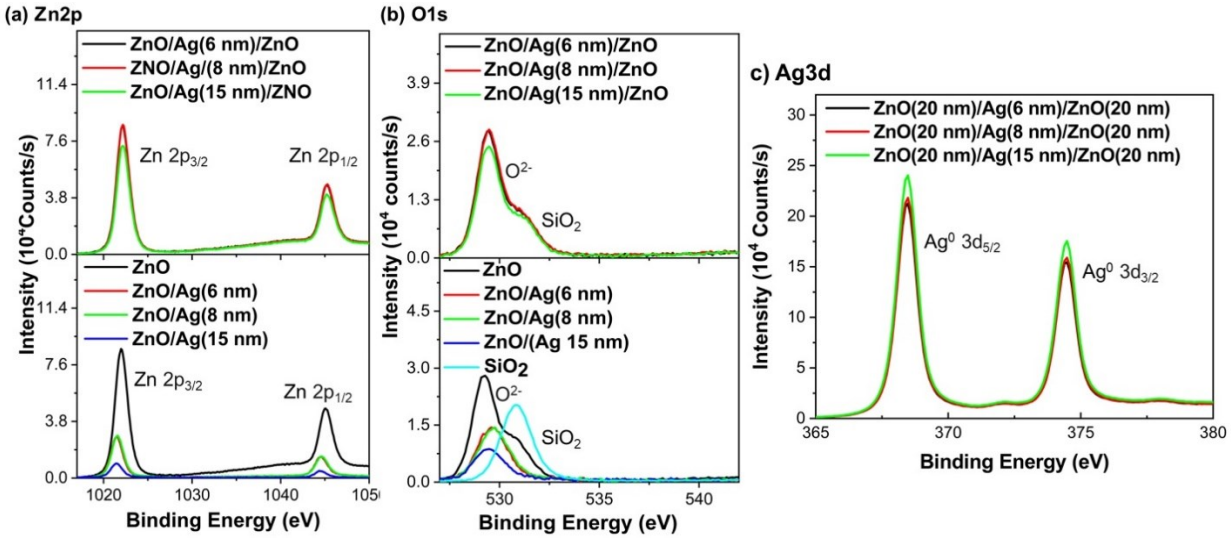

Figure 3. XPS spectra of the multilayers: (a) Zn 3d scan; (b) O1s scan; (c) Ag 3d scan.

The UPS spectra shown in Figure 4a,c give information on the electronic levels in the multilayer, with ZnO having a work function of 3.6 eV, which does not change for the multilayer ZnO/Ag (6 nm)/ZnO. For the multilayers with Ag thicknesses of 8 nm and 15 nm, the work function changes to 3.9 eV and 3.8 eV, respectively. UPS can give the minimum work function in a patchy nonuniform sample with a reported error of ± 0.05 eV and the maximum thickness that can be probed being about 40 nm.[29] On looking at the evolution of the work function of Ag on 20 nm of ZnO (Fig. S1), it is apparent that, on adding 6 nm of Ag, the work function increases to 4.83 eV. With 8 nm of Ag, the work function remains at 4.83 eV, and with 15 nm of Ag it decreases slightly to ~4.66 eV, which is slightly higher than the work function of pristine Ag at ~ 4.4 eV. This could be indicative of the interaction between ZnO and Ag as it becomes more positively charged by donating electrons to ZnO. From the valence band spectra in Figure 4b and Figure S3b, the peaks located around ~5 eV can be attributed to both O 2p orbitals and hybridized O 2p/Zn 4s orbitals, while the peaks around ~11 eV can be due to the Zn 3d band[2, 30]. There is a clear shift in both the intensities and the binding energy positions of the O 2p peaks for pristine ZnO film which occurs at 6.4eV which moves to 4.6 eV in the presence of Ag. While the hybridized O2p orbitals shift from 11.4eV for pristine ZnO to 10.8 eV with increased intensity for ZnO/Ag(6 nm), 10.7eV for ZnO/Ag/(8 nm) and the peak broadens and because very less intense for ZnO/Ag(15 nm) due to the increasing Ag thickness covering the ZnO. On adding another layer of 20 nm of ZnO there is less of a dramatic shift with the O2p hybridized peak shifting to lower binding energies as the thickness of the Ag sandwiched in between increases. It shifts from 6.6 eV to 5.9 eV while the O2p hybridized peaks remains around the same position at 11.5 eV. The Ag 4d peaks occur around 4-8eV[31, 32] which could be the reason the O2p shifts to the lower binding energy on adding Ag to ZnO. We expect the metallic Ag 5sp states near 0eV which is very faint here in the spectra appearing as a very weak peak at 0.6 eV. This can indicate charge transfer to the ZnO atoms. Once the curves are linearly fitted, the straight-line

intersection points against the baseline will give the onset of photoexcitation which is the valence band (VB) onset, Ev, in relation to the fermi energy level[30]. The VB onset for pristine ZnO is 2.00 eV which moves to 2.78 eV for 6 nm of Ag and 2.32 for 8 nm of Ag and 2.30 for 15 nm. On adding 20 nm of ZnO to these layers the VB onset reduces to 2.29eV for 6 nm of Ag, 2.3eV for 8 nm of Ag and 2.26 eV for 15 nm of Ag which shows more n-type behavior compared to the pristine ZnO. Taking the constraints and resolution of the UPS measurements and PL spectra into account we can conclude that the band alignment and electronic properties are brought out by interface states formed upon the metal deposition and not really by a fermi level pinning of the oxygen vacancies[31, 33, 34].

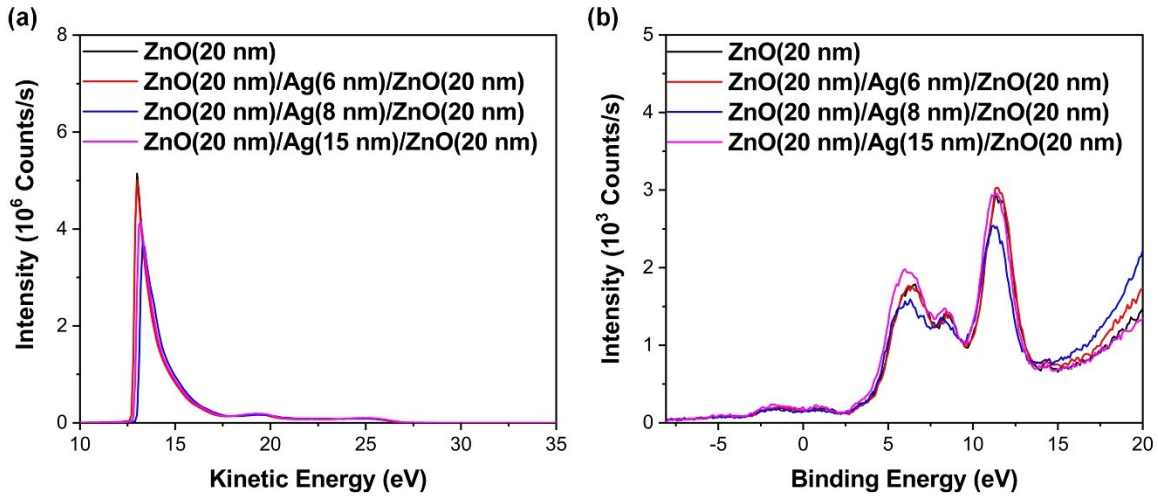

Figure 4. UPS spectra of the optimized multilayers with (a) work function measurements, (b) valence band measurements

Transparent OLED devices incorporating the optimized ZnO/Ag/ZnO multilayer TCE as the top contact were fabricated on ITO/glass and the emission and devices performance parameters were collected. Figure 5a,b show the energy level diagram and device layer structure used for the transparent OLEDs. The charge injection barrier for electron injection from the multilayer TCE to the emissive layer is estimated at 0.5 eV. A well-known solution-processed active layer composed of PFO:F8BT is employed.

The luminance is measured to be effectively the same for the emission from both sides of the device. The transparent OLED device has a turn-on voltage of 4.3 V and the EQE, power efficiency and current 05efficiency reach values of 8.6%, 2.75 lm/W and ~2.9 cd/A at 14.5 V (Figure 6). The EL spectra from the ZnO/Ag/ZnO side are broader than from the ITO side (Figure 5c), which corresponds to higher transmission in the 500 nm to 600 nm range (also visible in the transmission spectra in Figure 1). The broadening is also visible in the PL spectra where the F8BT peak is slightly broader from the ZnO/Ag/ZnO side (Figure 5d). In both PL spectra there is an incomplete charge transfer from PFO to F8BT visible from the appearance of the PFO peaks at 439 nm and 467 nm, which disappears in the EL spectrum showing only the peak for F8BT at ~534 nm from the ITO side, which shifts to 540 nm from the ZnO/Ag/ZnO side. Table 2 summarizes the OLED performance parameters in this work and alongside parameters reported in other published OLED studies that used multilayer TCEs. From this, we can see that although the transparent, solution-processed OLED device structure in this work has fewer layers compared the other OLEDs (comprising of just an anode, hole-transport layer (HTL), emissive layer (EML), and a multilayer TCE that serves as both and electron transport layer and cathode), and despite an injection barrier of 0.5 eV (Figure 5a), we still obtain a good current efficiency and maximum luminance of 3621 cd/m^2 at 18 V. This is mainly attributed to the very low sheet resistance, which is the lowest compared to the other multilayer TCEs used for OLED, and the high optical transmittance, which is one of the highest compared to the other reported multilayer TCEs used for OLEDs. While some of the devices on the table perform better than the devices in this work, they have more complex layer structure - made up of several HTL, ETL and buffer layers to bring down the barrier for charge injection and improve the charge transport properties. Most of them are also vacuum deposited, which also improves the overall device performance.

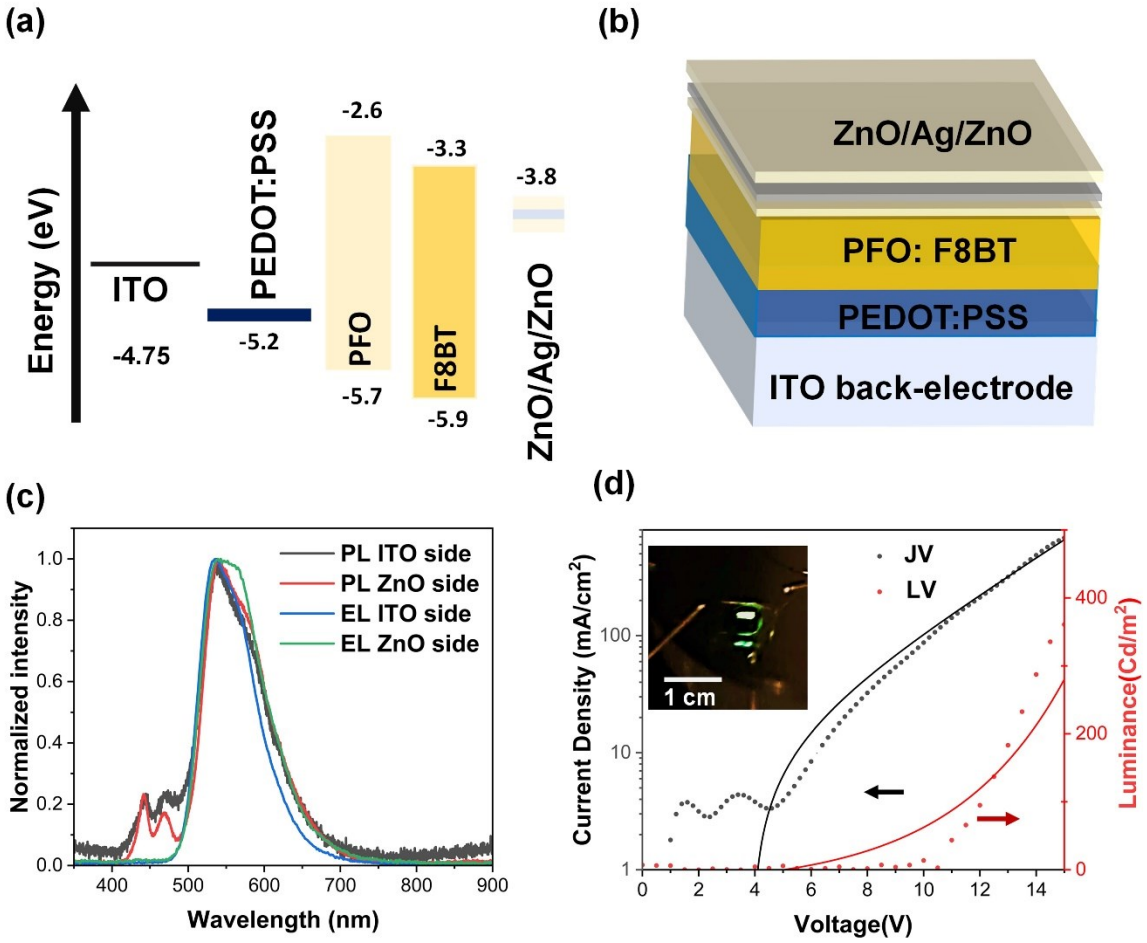

Figure 5. (a) The energy diagram of a bottom-emitting OLED device with ZnO/Ag/ZnO as the transparent (n-type) top-contact. (b) Schematic of the overall transparent OLED device structure. (c) EL and PL spectra of from fabricated devices with this structure. (d) JV and LV curves.

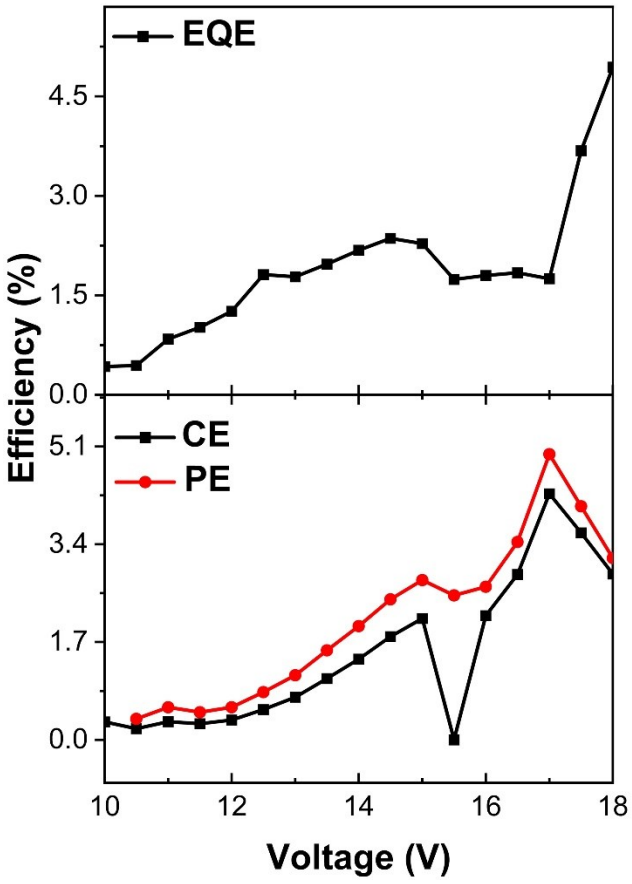

Figure 6. External quantum efficiency (EQE), current efficiency (CE) and power efficiency (PE) and versus voltage curves.

Table 2. Performance of the OLED devices in this work compared to OLEDs in other reports with metal oxide and Ag-based multilayer TCEs. For this work, the maximum luminance (L_{max}), currently efficiency (CE), and power efficiency (PE) are calculated from the sum of the luminance measured from the top and bottom sides of the device.

Type of electrode	**L_{max} (Cd/m^2)**	**CE at L_{max} (Cd/A)**	**Active layer deposition**	**Emission type**	**Polarity of the TCE**	**Sheet Resistance (Ω/□)**	**% Transmission**

ZnO/Ag/ZnO (this work)	3621 1153	3.6	Solution processed	Transparent	n-type	1.47	85
ZnS/Cs_2CO_3/ Ag/ZnS[35]	1500	3	Vacuum deposited	Transparent	n-type	8.38	74
ZnO/Mg:Ag/ ZnO[19]	43930	39.04	Vacuum deposited	Transparent	n-type	11.7	86
MoO_3/Ag/Mo O_3[36]	29148	11.5	Solution processed	Transparent	Act as both p-type and n-type	~15	76
ZnO/Ag/ZnO /Ag/WO[37]	~2000 at 80 ma/cm^2	~3.25	Vacuum deposited	Bottom emitting	p-Type	1.6	75
ZnS/Ag/ZnO/ Ag/WO_3[38]	10000	2.5 Lm/W	Vacuum deposited	Bottom emitting	p-type	2.17	82
Zno/Ag/ZnO[18]	18713	17.58	Vacuum deposited	Bottom emitting	p-type	1.6	80
ZnO/Ag/ZnO [20]	855.2	5.8	Vacuum Deposited	Bottom emitting	P-type	10.3	~95
Ni doped ZnO/Ag/ZnO [20]	1157.3	17.2	Vacuum deposited	Bottom emitting	p-type	6.33	93

Overall, the comparison in Table 2 shows that there is good potential for further studies using our TCE system in top-emitting and transparent OLEDs. Our methods also involves a sputtering technique that causes minimal damage to the active layer and that can easily be adapted to the vacuum deposition processes. The efficiency of these transparent OLED devices can be further improved by adding additional charge transport materials to improve charge injection and charge balance, and by vacuum

depositing the active layer. Studies on different doping techniques for better energy level alignment is also expected to further optimize the performance of the TCE in the device.

4. Conclusion

We have demonstrated a n-type transparent conducting electrode deposited by low power sputtering that can be used for top-emitting and transparent OLEDs. The n-type transparent electrode was composed of a layer of silver sandwiched in between two zinc oxide layers and was deposited directly on the OLED emissive layer without notable degradation. Tuning the electrical properties and transmission enabled multilayer optical and electronic characteristics that approach that of ITO. The work function of the multilayer was found to be suitable for a n-type charge transport throughout the multilayer and the operation of the TCE was demonstrated in a transparent OLED.

5. Acknowledgements

The authors are grateful to Prof. Sylvie Rangan for her assistance with Ultraviolet Photoelectron Spectroscopy and X-ray Photoelectron Spectroscopy. The authors acknowledge the support of Nanofabrication Core facility (NCF), Rutgers University for providing experimental facilities for this investigation, and TechAdvance (TA2021-0031) funding from the Rutgers' Office of Innovation Ventures and National Science Foundation (NSF) (2314068) for providing the funding for the project. VB and VP acknowledge the support of their research at Rutgers University via the Donald H. Jacobs Chair in Applied Physics.

6. References

(1) Wei, M.; Li, C.-F.; Deng, X.-R.; Deng, H. Surface Work Function of Transparent Conductive ZnO Films. *Energy Procedia* **2012**, *16*, 76-80. DOI: https://doi.org/10.1016/j.egypro.2012.01.014.
(2) Drewelow, G.; Reed, A.; Stone, C.; Roh, K.; Jiang, Z.-T.; Truc, L. N. T.; No, K.; Park, H.; Lee, S. Work function investigations of Al-doped ZnO for band-alignment in electronic and optoelectronic applications. *Applied Surface Science* **2019**, *484*, 990-998. DOI: https://doi.org/10.1016/j.apsusc.2019.04.079.
(3) Klein, A.; Körber, C.; Wachau, A.; Säuberlich, F.; Gassenbauer, Y.; Harvey, S. P.; Proffit, D. E.; Mason, T. O. Transparent Conducting Oxides for Photovoltaics: Manipulation of Fermi Level, Work Function and Energy Band Alignment. In *Materials*, 2010; Vol. 3, pp 4892-4914.
(4) Girtan, M. Comparison of ITO/metal/ITO and ZnO/metal/ZnO characteristics as transparent electrodes for third generation solar cells. *Solar Energy Materials and Solar Cells* **2012**, *100*, 153-161. DOI: https://doi.org/10.1016/j.solmat.2012.01.007.
(5) Kim, J. H.; Kang, T.-W.; Na, S.-I.; Yoo, Y.-Z.; Seong, T.-Y. ITO-free inverted organic solar cells fabricated with transparent and low resistance ZnO/Ag/ZnO multilayer electrode. *Current Applied Physics* **2015**, *15* (7), 829-832. DOI: https://doi.org/10.1016/j.cap.2015.05.001.
(6) Sharma, V.; Kumar, P.; Kumar, A.; Surbhi; Asokan, K.; Sachdev, K. High-performance radiation stable ZnO/Ag/ZnO multilayer transparent conductive electrode. *Solar Energy Materials and Solar Cells* **2017**, *169*, 122-131. DOI: https://doi.org/10.1016/j.solmat.2017.05.009.
(7) Xu, R.; Yang, K.; Zang, Y. ZnO/Ag/ZnO multilayer transparent electrode for highly-efficient ITO-Free polymer solar cells. *Current Applied Physics* **2020**, *20* (3), 425-430. DOI: https://doi.org/10.1016/j.cap.2020.01.003.
(8) Takaloo, A. V.; Lee, H. J.; Park, T. H.; Dongale, T. D.; Kim, Y. U.; Choi, D. H.; Kim, T. G. Haze-enhanced ZnO/Ag/ZnO nanomesh electrode for flexible, high-efficiency indoor organic photovoltaics. *Journal of Power Sources* **2021**, *515*, 230589. DOI: https://doi.org/10.1016/j.jpowsour.2021.230589.
(9) Kim, A.; Won, Y.; Woo, K.; Kim, C.-H.; Moon, J. Highly Transparent Low Resistance ZnO/Ag Nanowire/ZnO Composite Electrode for Thin Film Solar Cells. *ACS Nano* **2013**, *7* (2), 1081-1091. DOI: 10.1021/nn305491x.
(10) Chalh, M.; Vedraine, S.; Lucas, B.; Ratier, B. Plasmonic Ag nanowire network embedded in zinc oxide nanoparticles for inverted organic solar cells electrode. *Solar Energy Materials and Solar Cells* **2016**, *152*, 34-41. DOI: https://doi.org/10.1016/j.solmat.2016.03.021.
(11) Sahu, D. R.; Lin, S.-Y.; Huang, J.-L. ZnO/Ag/ZnO multilayer films for the application of a very low resistance transparent electrode. *Applied Surface Science* **2006**, *252* (20), 7509-7514. DOI: https://doi.org/10.1016/j.apsusc.2005.09.021.
(12) Mohamed, S. H. Effects of Ag layer and ZnO top layer thicknesses on the physical properties of ZnO/Ag/Zno multilayer system. *Journal of Physics and Chemistry of Solids* **2008**, *69* (10), 2378-2384. DOI: https://doi.org/10.1016/j.jpcs.2008.03.019.
(13) Jiang, C. Y.; Sun, X. W.; Zhao, D. W.; Kyaw, A. K. K.; Li, Y. N. Low work function metal modified ITO as cathode for inverted polymer solar cells. *Solar Energy Materials and Solar Cells* **2010**, *94* (10), 1618-1621. DOI: https://doi.org/10.1016/j.solmat.2010.04.082.
(14) Lee, B. R.; Goo, J. S.; Kim, Y. W.; You, Y.-J.; Kim, H.; Lee, S.-K.; Shim, J. W.; Kim, T. G. Highly efficient flexible organic photovoltaics using quasi-amorphous ZnO/Ag/ZnO transparent electrodes for indoor applications. *Journal of Power Sources* **2019**, *417*, 61-69. DOI: https://doi.org/10.1016/j.jpowsour.2019.02.015.
(15) Klöppel, A.; Kriegseis, W.; Meyer, B. K.; Scharmann, A.; Daube, C.; Stollenwerk, J.; Trube, J. Dependence of the electrical and optical behaviour of ITO–silver–ITO multilayers on the silver

properties. *Thin Solid Films* **2000**, *365* (1), 139-146. DOI: https://doi.org/10.1016/S0040-6090(99)00949-9.
(16) Chen, P. S.; Peng, C.-H.; Chang, Y.-W.; Lin, T. W.; Lee, S. W. Improved Indium-Free Transparent ZnO/Metal/ZnO Electrode through a Statistical Experimental Design Method. *Advances in Materials Science and Engineering* **2016**, *2016*, 7258687. DOI: 10.1155/2016/7258687.
(17) Kusano, E.; Kawaguchi, J.; Enjouji, K. Thermal stability of heat-reflective films consisting of oxide–Ag–oxide deposited by dc magnetron sputtering. *Journal of Vacuum Science & Technology A* **1986**, *4* (6), 2907-2910. DOI: 10.1116/1.573658 (acccessed 4/5/2024).
(18) Liu, Y.; Ding, T.; Wang, H.; Zhang, Y.; Chen, C.; Chen, X.; Duan, Y. Improved injection properties of self-passivated degenerated transparent electrode for organic and perovskite light emitting devices. *Applied Surface Science* **2020**, *504*, 144442. DOI: https://doi.org/10.1016/j.apsusc.2019.144442.
(19) Chen, X.; Wu, D.; Wang, J.; Zhou, Y.; Zhang, Z.; Li, C.; Zhang, J.; Chen, P.; Duan, Y. A highly transparent laminated composite cathode for organic light-emitting diodes. *Applied Physics Letters* **2021**, *119* (7). DOI: 10.1063/5.0057184 (acccessed 4/5/2024).
(20) Kyu Kang, S.; Yun Kang, D.; Wan Park, J.; Rock Son, K.; Geun Kim, T. Work function-tunable ZnO/Ag/ZnO film as an effective hole injection electrode prepared via nickel doping for thermally activated delayed fluorescence-based flexible blue organic light-emitting diodes. *Applied Surface Science* **2021**, *538*, 148202. DOI: https://doi.org/10.1016/j.apsusc.2020.148202.
(21) Chen, S.; Deng, L.; Xie, J.; Peng, L.; Xie, L.; Fan, Q.; Huang, W. Recent Developments in Top-Emitting Organic Light-Emitting Diodes. *Advanced Materials* **2010**, *22* (46), 5227-5239. DOI: https://doi.org/10.1002/adma.201001167.
(22) Chen, Y.; Yi, H. T.; Podzorov, V. High-Resolution ac Measurements of the Hall Effect in Organic Field-Effect Transistors. *Physical Review Applied* **2016**, *5*. DOI: 10.1103/PhysRevApplied.5.034008.
(23) He, X.; Qian, H.; Zhi, Q.; Zhang, M.; Luo, J.; He, R.; Zeng, Q. Investigation on the enhancement of ultraviolet emission in Ag-ZnO microrods. *Applied Surface Science* **2013**, *283*, 571-576. DOI: https://doi.org/10.1016/j.apsusc.2013.06.147.
(24) Ma, S. Y.; Yang, X. H.; Huang, X. L.; Sun, A. M.; Song, H. S.; Zhu, H. B. Effect of post-annealing treatment on the microstructure and optical properties of ZnO/PS nanocomposite films. *Journal of Alloys and Compounds* **2013**, *566*, 9-15. DOI: https://doi.org/10.1016/j.jallcom.2013.02.179.
(25) Chopra, K. L.; Bahl, S. K. Hall Effect in Thin Metal Films. *Journal of Applied Physics* **2004**, *38* (9), 3607-3610. DOI: 10.1063/1.1710180 (acccessed 1/24/2024).
(26) Sondheimer, E. H. The Influence of a Transverse Magnetic Field on the Conductivity of Thin Metallic Films. *Physical Review* **1950**, *80* (3), 401-406. DOI: 10.1103/PhysRev.80.401.
(27) Anand, A.; Islam, M. M.; Meitzner, R.; Schubert, U. S.; Hoppe, H. Introduction of a Novel Figure of Merit for the Assessment of Transparent Conductive Electrodes in Photovoltaics: Exact and Approximate Form. *Advanced Energy Materials* **2021**, *11* (26), 2100875. DOI: https://doi.org/10.1002/aenm.202100875.
(28) Fraser, D. B.; Cook, H. D. Highly Conductive, Transparent Films of Sputtered In2 − x Snx O 3 − y. *Journal of The Electrochemical Society* **1972**, *119* (10), 1368. DOI: 10.1149/1.2403999.
(29) Sreekumar, S.; Heidari, M.; Cheng, Z.; Maddali, H.; House, K.; Frei, H.; Galoppini, E.; O'Carroll, D. M. Self-Assembled Monolayers for Improved Charge Injection of Silver Back Electrodes in Inverted Organic Electronic Devices. *ACS Applied Materials & Interfaces* **2022**, *14* (33), 38270-38280. DOI: 10.1021/acsami.2c07610.
(30) Joshi, A. G.; Sahai, S.; Gandhi, N.; Krishna, Y. G. R.; Haranath, D. Valence band and core-level analysis of highly luminescent ZnO nanocrystals for designing ultrafast optical sensors. *Applied Physics Letters* **2010**, *96* (12). DOI: 10.1063/1.3354025 (acccessed 1/24/2024).

(31) Chernysheva, E.; Srour, W.; Philippe, B.; Baris, B.; Chenot, S.; Duarte, R. F.; Gorgoi, M.; Cruguel, H.; Rensmo, H.; Montigaud, H.; et al. Band alignment at Ag/ZnO(0001) interfaces: A combined soft and hard x-ray photoemission study. *Physical Review B* **2018**, *97* (23), 235430. DOI: 10.1103/PhysRevB.97.235430.
(32) Ozawa, K.; Sato, T.; Kato, M.; Edamoto, K.; Aiura, Y. Angle-Resolved Photoemission Spectroscopy Study of Adsorption Process and Electronic Structure of Silver on ZnO(10$\bar{1}$0). *The Journal of Physical Chemistry B* **2005**, *109* (30), 14619-14626. DOI: 10.1021/jp051975e.
(33) Monakhov, E. V.; Kuznetsov, A. Y.; Svensson, B. G. Zinc oxide: bulk growth, role of hydrogen and Schottky diodes. *Journal of Physics D: Applied Physics* **2009**, *42* (15), 153001. DOI: 10.1088/0022-3727/42/15/153001.
(34) Allen, M. W.; Durbin, S. M. Influence of oxygen vacancies on Schottky contacts to ZnO. *Applied Physics Letters* **2008**, *92* (12). DOI: 10.1063/1.2894568 (acccessed 1/24/2024).
(35) Kim, D.-Y.; Han, Y. C.; Kim, H. C.; Jeong, E. G.; Choi, K. C. Highly Transparent and Flexible Organic Light-Emitting Diodes with Structure Optimized for Anode/Cathode Multilayer Electrodes. *Advanced Functional Materials* **2015**, *25* (46), 7145-7153. DOI: https://doi.org/10.1002/adfm.201502542.
(36) Ko, K.-J.; Cho, H. W.; Lee, H. B.; Jesuraj, P. J.; Kang, J.-W.; Ryu, S. Y. Indium-free, highly flexible semi-transparent organic light-emitting diodes featuring MoO3/Au/MoO3 multilayer anode and cathode. *Organic Electronics* **2024**, *128*, 107022. DOI: https://doi.org/10.1016/j.orgel.2024.107022.
(37) Lee, S.-M.; Choi, C. S.; Choi, K. C.; Lee, H.-C. Low resistive transparent and flexible ZnO/Ag/ZnO/Ag/WO3 electrode for organic light-emitting diodes. *Organic Electronics* **2012**, *13* (9), 1654-1659. DOI: https://doi.org/10.1016/j.orgel.2012.05.014.
(38) Yang, D. Y.; Lee, S.-M.; Jang, W. J.; Choi, K. C. Flexible organic light-emitting diodes with ZnS/Ag/ZnO/Ag/WO3 multilayer electrode as a transparent anode. *Organic Electronics* **2014**, *15* (10), 2468-2475. DOI: https://doi.org/10.1016/j.orgel.2014.06.021.